

Effect of explosive emission on runaway electron generation

D. Levko,^{a)} S. Yatom, V. Vekselman, J. Z. Gleizer, V. Tz. Gurovich, and Ya. E. Krasik
Department of Physics, Technion, 32000 Haifa, Israel

(Received 28 July 2011; accepted 27 November 2011; published online 11 January 2012)

The results of numerical simulations of the generation of runaway electrons in a nitrogen-filled coaxial diode with electron emission governed by field emission that transfers to explosive emission with a variable time delay are presented. It is shown that the time when the explosive emission turns on influences significantly the generation of runaway electrons. Namely, an explosive emission turn-on prior to the formation of the virtual cathode leads to an increase in the current amplitude of the runaway electrons and a decrease in its duration. Conversely, an explosive emission turn-on after the formation of the virtual cathode and during the high-voltage pulse rise time does not influence the generation of runaway electrons significantly. When the explosive emission turns on during the fall of the high-voltage pulse and after the virtual cathode formation, one obtains additional runaway electron generation. Finally, a comparison between electron energy distributions obtained with and without explosive emission turn-on showed that the former increases the number of electrons in the high-energy tail and the electrons' largest energy. The comparison of both the simulated electron energy distributions with the experimentally obtained electron spectrum has shown that the best fit is obtained when the explosive emission is considered in the simulation.

© 2012 American Institute of Physics. [doi:10.1063/1.3676198]

I. INTRODUCTION

Today, sub-nanosecond pulsed high-voltage (HV) and high-current discharges in pressurized gases are applied in plasma-assisted combustion,¹ pulsed gaseous lasers,² the generation of electron beams, x-rays,³ etc. It is known⁴ that HV nanosecond scale discharges in gases at high pressures propagate as a fast ionization wave (FIW) with a typical velocity of $\sim 10^9$ to 10^{10} cm/s. In order to describe the FIW propagation, the phenomenon of runaway electrons (RAEs) is considered.^{4–15} These RAEs efficiently generate secondary electrons and ions, which produce gas pre-ionization during their propagation toward the anode. In addition, secondary electrons participate in ionization processes, forming plasma that could result in the shorting of the cathode-anode (CA) gap.

FIW propagation has been studied using different numerical simulations (see, for instance, Refs. 5–13). Slavin and Sopin⁶ calculated the electron energy distribution function (EEDF) in a FIW by dividing the electrons into two groups: low-energy “plasma” electrons and high-energy “runaway” electrons. Low-energy electrons were studied using the hydrodynamic approach, and high-energy electrons were considered in the diffusion approximation solving the Boltzmann equation with an inelastic loss integral. Sinkevich and Trofimov⁵ and Boutine *et al.*⁷ developed a hydrodynamic model accounting for the space-charge of secondary electrons and ions that allows one to obtain the temporal and spatial evolution of the potential distribution. Namely, Boutine *et al.*⁷ considered the electron distribution in three macro-energetic groups when studying the breakdown of chlorine. The EEDF

for each group was described by a Maxwellian distribution with different mean energies. This approach allows one to consider separately the ionization processes produced by “fast” and “slow” electrons and to avoid their mixing during the averaging in the hydrodynamic approximation.

Starikovskaia and Starikovskii⁸ developed a numerical model of FIW propagation in nitrogen, but without accounting for the self space-charge of secondary electrons and ions. These simulations showed that the EEDF is overpopulated near the FIW front by high-energy electrons, the propagation of which toward the anode leads to effective gas pre-ionization and the acceleration of secondary electrons by a strong electric field existing at the FIW front. Behind the FIW front, the electric field weakened rapidly and the mean electron energy and directed electron velocity decreased gradually, whereas the electron density increased.

Another approach describing FIW propagation and RAE generation is based on Particle-in-Cell (PIC) numerical simulations. One of the first PIC simulations of RAE generation in pressurized gases was carried out by Kunhardt *et al.*⁹ In their work, electron avalanche propagation in an external electric field ($E \geq 6 \times 10^4$ V/cm) was studied, and the EEDF versus the distance from the cathode and avalanche dimensions were determined. However, these simulations did not consider electron field emission (FE) from the cathode and the influence of secondary electrons and ion space-charge on the external electric field.

In numerical simulations carried out by Yakovlenko *et al.* (see Ref. 12), RAE generation was studied for different electrode configurations (planar or cylindrical geometry), types of background gas, and accelerating voltage waveforms. The numerical simulations were carried out using one-dimensional Particle-in-Cell (1D PIC) code for planar electrode geometry. Also, these simulations did not consider

^{a)}Author to whom correspondence should be addressed. Electronic mail: dlevko@physics.technion.ac.il.

the changes in electric field distribution caused by the secondary electrons and ion space charge, and FE was not accounted for. It was shown that the breakdown of over-voltage gas-filled gaps could be described by the Townsend model only when the distance d_{CA} between the CA electrodes exceeded some critical length l_{cr} . In this case, the results of simulations showed that the maximum of the EEDF at the anode corresponds to electron energies $\varepsilon \ll e\varphi_c$, where φ_c is the cathode potential and e is the electron charge. When $l_{cr} > d_{CA}$, the Townsend model fails to describe the breakdown formation. In this case, the majority of the electrons were found to be accelerated continuously, forming RAEs, and the maximum of the EEDF was obtained at $\varepsilon \approx e\varphi_c$. It was shown that the volume discharge in a non-uniform electric field is developed by secondary electrons formed in the process of gas ionization by RAEs. In addition, these simulations showed that RAE generation occurs only near the cathode, where one obtains the largest electric field.

Mesyats *et al.*^{3,11} carried out numerical simulations of electron generation in a diode using PIC code, considering electric field enhancement at the cathode surface micro-protrusions and shielding of the external electric field by the space charge of FE electrons. However, these simulations did not account for inelastic collisions and the scattering of electrons propagating toward the anode.

Comprehensive simulations of RAE generation in a non-uniform electric field for the initial stage (a few tens of picoseconds) of the gas discharge were carried out by Shklyayev *et al.*¹³ The developed numerical model considers the shielding of the FE and the self-consistent electric field distribution, i.e., the effect of the space charge of the secondary electrons and ions and emitted electrons was accounted for. The simulations showed that RAE generation occurred in the vicinity of the cathode during a few tens of picoseconds. The termination of RAE generation occurs when the electric field produced by the space charge of emitted electrons screens the external electric field to a significant extent. Also, the influence of electric field enhancement by the cathode micro-protrusions and of the different work functions of the cathode material on the RAE parameters was studied. It was shown that in the case of a low work function, a large amount of emitted electrons, which are already generated efficiently during the HV pre-pulse, produce the plasma (secondary electrons and ions) at distances of less than a few hundreds of microns from the cathode. This plasma becomes the source of RAEs, which are emitted from its boundary during the main HV pulse. In addition, simulations showed the formation of a potential well that causes the capture of electrons with energies smaller than the plasma potential. In the opposite case (i.e., a large work function), the amount of FE electrons decreases, and plasma is not generated during the HV pre-pulse. Thus, RAE generation occurs only in the cathode vicinity. The results of these simulations of the initial stage of the gas discharge showed that RAEs consist of both FE electrons and secondary electrons generated in the vicinity of the cathode.

In spite of numerous experimental, numerical, and theoretical investigations of RAE generation, there is no complete understanding of the processes that determine the RAE

parameters; that is, the processes that accompany RAE formation and such issues as the locations of RAE generation and its termination are not yet well understood. As mentioned above, numerical simulations¹³ have shown that RAE formation is terminated when the space charge of secondary electrons becomes sufficient to screen the applied electric field at the cathode surface. Another explanation for RAE termination is suggested by the results of numerical simulations¹⁶ that showed that the RAE parameters are determined by the formation of the virtual cathode (VC) in the CA gap. Namely, the formation of the VC terminates RAE generation from the region in the vicinity of the cathode. However, the VC itself could become the source of RAEs if the electric field at its location toward the anode becomes larger than critical electric field E_{cr} .^{2,3} The origin of RAE—i.e., whether FE, explosive emission (EE), or secondary electrons are the source of these electrons—is still a debatable issue. For instance, Mesyats *et al.*¹¹ reported that RAE generation could be terminated when FE transfers to EE.

This paper presents the results of 1D PIC numerical simulations of the EE influence on RAE generation in molecular nitrogen (N_2) at atmospheric pressure. It is shown that, indeed, the time of EE switching influences significantly RAE parameters such as the time duration, locations of its generation, and the EEDF.

II. NUMERICAL MODEL

In order to simulate the generation of RAEs in pressurized N_2 gas, a 1D PIC numerical code¹⁶ was used. In the model, the coaxial diode geometry was considered (cathode with a radius of 3 μm and anode with a radius of $r_{CA} = 1$ cm). This diode configuration allows one to consider the enhancement of the cathode electric field that is typical for diodes with blade-like cathodes. The radial distance-velocity phase space is divided into elementary cells with dimensions dr and dv . At each time interval, the system of equations for electron propagation in the local electric field was solved numerically.¹⁷ In order to follow the energy conservation law, first new coordinates of electrons were calculated. Next, at the same time interval dt , the electrons' energy was calculated using new and old electron coordinates and the local electric field value that was calculated at the preceding time interval. The sequence of numerical simulations is shown in Fig. 1.

The probability of collisions between neutrals and electrons in the cell was defined as¹²

$$P = 1 - \exp[-\Delta r/\lambda(\varepsilon)]. \quad (1)$$

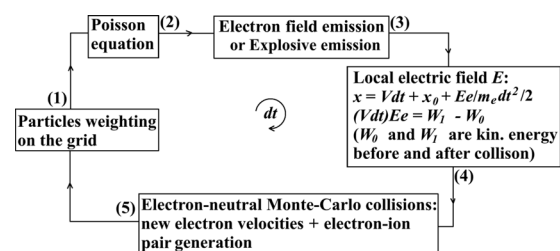


FIG. 1. The sequence of numerical simulations.

Here, Δr is the distance over which electrons propagate during one time step, and $\lambda(\varepsilon)$ is the mean free path of electrons in N_2 gas. In the calculations of λ , the elastic scattering cross section σ_{el} of electrons by neutrals and the inelastic collision cross sections (ionization cross-section σ_{ion} and excitation cross section of the first electronic energy level of N_2 σ_{ex}) were accounted for, resulting in the total mean free path

$$\lambda(\varepsilon) = \frac{1}{N \cdot [\sigma_{el}(\varepsilon) + \sigma_{ion}(\varepsilon) + \sigma_{ex}(\varepsilon)]}. \quad (2)$$

Here N is the density of neutrals. The type of collision was defined by the ratio between cross sections of the considered processes. The NIST database¹⁸ was used for the ionization cross section of N_2 and elastic scattering. The excitation and elastic scattering cross sections were extrapolated for high energies (up to 200 keV) using the values of cross sections presented in Ref. 19. In addition, electron scattering forward and backward in both elastic and inelastic processes was considered.¹² The direction of the electron propagation after the collision was defined by the sign of the expression that determines the scattering angle χ ,²⁰

$$\cos \chi = 1 - 2 \cdot \varepsilon_1 \cdot \left[(1 + \varepsilon/\varepsilon_1)^{rnd} - 1 \right] / \varepsilon, \quad (3)$$

where $\varepsilon_1 = 1$ eV is the characteristic scattering energy and rnd is a random number ($0 \leq rnd < 1$) that was used in the Monte Carlo subroutine. Only two dimensions in phase space were considered in the numerical model, namely, the propagation along the radius of the coaxial cylindrical diode and the radial velocity. Therefore, if the sign of $\cos \chi$ remains positive, electrons continue propagating toward the anode. Otherwise, electrons move backward after the collision. The value of $\cos \chi$ was used to define the energy losses of electrons in the radial direction as a result of the change in the absolute value of the radial velocity vector. The use of Eq. (3) for the definition of the scattering angle is still debatable (see Refs. 20–22). For instance, Phelps²¹ proposed another equation to define the scattering angle,

$$\cos \chi = \frac{1 - \beta(\varepsilon) - rnd}{1 - \beta(\varepsilon) - rnd + 2 \cdot \beta(\varepsilon) \cdot rnd}, \quad (4)$$

where $\beta(\varepsilon)$ is a screening parameter depending on the electron's energy and type of collision. However, the comparison between Eqs. (3) and (4) showed that at $\varepsilon < 100$ eV, calculated angles are in satisfactory agreement for all values of rnd for both elastic and inelastic collisions. At larger electron energies, the scattering angles obtained by Eqs. (3) and (4) become different for elastic collisions at $rnd > 0.9$ and for inelastic collisions at $rnd > 0.6$. Nevertheless, these discrepancies in scattering angles are not crucial, because the probability of electron-neutral collisions calculated by Eq. (1) decreases drastically for high-energy electrons. Thus, the use of Eq. (3) for the calculation of the scattering angle can be considered as a satisfactory approximation.

In each process of molecule ionization, one electron-ion pair is generated. The newly generated secondary electron is added to the primary electrons. The velocities of the

secondary electron and ion are assumed to be zero, and their location is determined by the coordinate of the primary ionizing electron. In the model, the ions' motion was taken into account as well. Depending on the initial conditions, the time interval dt was varied in the range of 10^{-15} to 10^{-14} s, allowing electrons to propagate $\Delta r \ll \lambda$ during dt . Because of the strongly inhomogeneous electric field, the space step was $\approx 10^{-7}$ m.

The radial potential distribution was calculated by solving the Poisson equation at the beginning of each time step for new electron and ion space charge distributions and new boundary conditions.

$$\frac{1}{r} \frac{d}{dr} \left(r \frac{d\varphi(r,t)}{dr} \right) = - \frac{\rho_i(r,t) - \rho_e(r,t)}{\varepsilon_0}. \quad (5)$$

Here, $\varphi(r,t)$, $\rho_i(r,t)$, and $\rho_e(r,t)$ are the potential, ion, and electron space charge densities, respectively, at a given time t at a distance r from the cathode. Here let us note that in general, the variation in the diode current changes the diode voltage amplitude and waveform because of the finite internal impedance of the pulsed generator. In the developed model, this process, which is specific for each generator, was not accounted for. Namely, a simplified electrical circuit that allows one to obtain a sine-like cathode potential was considered. Equation (5) was solved with the cathode and anode boundary conditions for potential.

$$\varphi_c = -\varphi_0 \sin\left(\frac{2\pi t}{T}\right), \varphi_a = 0. \quad (6)$$

Here, $\varphi_0 = 120$ kV is the maximal cathode potential. The rise time of the cathode potential was determined as $T/4$, where T is the period that was varied as 1 ns or 2 ns.

In earlier research (see Refs. 3, 11–13, and 17), only the FE of electrons from the cathode governed by the Fowler-Nordheim (FN) law²³ was considered. In this work, the electron emission from the cathode was a uniform FE until it was switched to EE. The cathodes used in experiments have micro-protrusions, and their distribution at the cathode surface, number, density, and micro-protrusion apex dimensions are undefined variables that could be varied even during a single generator shot. Due to the large electric field enhancement at the apexes, these micro-protrusions could significantly change the parameters of the FE. However, one can consider two competing processes for the FE of electrons from micro-protrusions. Firstly, the smaller cross-sectional area of the micro-protrusions' apexes leads to a smaller quantity of emitted electrons. Secondly, the number of electrons emitted from each micro-protrusion is significantly larger than from the wire for the same micro-protrusion apex area, due to a larger electric field enhancement at the micro-protrusion's apex for the same potential value. These two competitive processes allow one to decrease the inaccuracy related to the concern of a uniform FE from the cathode.

According to the model, at the beginning of each time step, a quantity dN_{em} of electrons with zero velocity and zero (cathode) coordinates was added to the simulations in accordance with the FN law. The value of dN_{em} was

determined as $dN_{em} = j_{FN} \cdot S \cdot dt/e$, where j_{FN} is the electron current density, dt is the time step, e is the electron charge, and S is the cathode surface area. In Refs. 11, 14, and 24, it was considered that RAE generation could be terminated when the FE transfers to EE. This transfer begins when the action integral reaches a critical value, i.e., when $\int^2 t_d \approx \bar{h}$, where t_d is the time delay of the cathode explosion, i.e., the beginning of the EE, and \bar{h} is the specific action of the metal explosion (for iron, $\bar{h} = 1.4 \times 10^9 \text{ A}^2 \text{ s cm}^{-4}$).²⁵ Simulations have shown that in the considered model, the highest value of FE current density did not exceed a value of 10^8 A/cm^2 and $t_d > 10^{-7} \text{ s}$. Therefore, the EE should never start for the considered voltage rise time (0.25–0.5 ns). Nevertheless, experiments²⁶ have shown that the generation of RAEs during sub-nanosecond discharges is accompanied by the appearance of micro-craters on the cathode surface. The appearance of these micro-craters strongly indicates that the cathode micro-protrusions have exploded. The current density from these micro-protrusions could be $>10^9 \text{ A/cm}^2$, and the value of t_d becomes significantly lower than 1 ns HV pulse duration.

The micro-protrusions on the cathode surface cannot be considered within the 1D model. Therefore, in order to simulate the influence of EE on the RAE generation, the time t_d was considered as a parameter with three typical values, namely, prior to and after the VC formation and close to the time of VC formation. According to the model, the EE switching terminates FE, and EE was simulated from the boundary of the cathode plasma having cathode potential and propagating toward the anode with an ion-sound velocity $V_C = 2 \times 10^4 \text{ m/s}$.²⁵ The processes inside the cathode plasma were not considered. The number of emitted electrons at each time step was defined so as to satisfy zero electric field at the plasma boundary. Uniformly emitted electrons with initial velocities²⁵ of 10^6 m/s were added into the numerical cell closest to the cathode. In addition, it was taken into account that the plasma propagation along the cell deletes a part of the electrons and ions from that cell. The numbers of those electrons and ions were proportional to the ratio between the cross-sectional areas of the rings with thicknesses of $V_C dt$ and dr , respectively.

III. RESULTS AND DISCUSSION

Simulations have shown that FE injects the first electron into the CA gap when the electric field at the cathode $E_c \geq 2 \times 10^7 \text{ V/cm}$. For example, for $\varphi_0 = 120 \text{ kV}$, $T = 1 \text{ ns}$, and $r_{CA} = 1 \text{ cm}$, one obtains $E_c \approx 2 \times 10^7 \text{ V/cm}$ at $t \approx 60 \text{ ps}$ when the cathode potential is $\varphi_C \approx 44 \text{ kV}$. Therefore, for

$\varphi_0 = 120 \text{ kV}$ and $T = 1 \text{ ns}$, the simulations were started at $t \geq 60 \text{ ps}$. In Ref. 11, it is reported that time $t_d \approx 100 \text{ ps}$ is required for the current to heat and explode micro-protrusions, i.e., for the beginning of EE. Because these micro-protrusions on the cathode surface are not included in the 1D model, the value of t_d is considered as a parameter. According to earlier research,¹⁶ the time evolution of the potential distribution in the CA gap has three typical stages. During the first stage, the space charge of secondary electrons and ions does not influence the external electric field significantly. For $\varphi_0 = 120 \text{ kV}$ and $T = 1 \text{ ns}$, this stage continues during $\Delta t \approx 20 \text{ ps}$ with respect to the beginning of FE. During the second stage, the vacuum potential distribution becomes disturbed by the increased space charge of these secondary electrons and ions generated in the CA gap. The spatial separation between electrons and ions causes the VC formation. The main part of the electrons in the VC location have energies smaller than the ionization potential of N_2 , and these electrons cannot generate new electron-ion pairs. In addition, the ions did not propagate significantly toward the VC to neutralize it because of a short time in the rise of the cathode potential. The third stage takes place when the VC is formed in the CA gap. Depending on the initial conditions (T , φ_0 , working gas, etc.), the time of the VC's formation varies in the range of $t_{VC} \approx 120 \text{ ps}$ to 300 ps (for instance, for $\varphi_0 = 120 \text{ kV}$ and $T = 1 \text{ ns}$, $t_{VC} \approx 123 \text{ ps}$). Thus, the EE could be switched on either at $t_d < t_{VC}$ or at $t_d > t_{VC}$. Therefore, further simulations for $\varphi_0 = 120 \text{ kV}$ and $T = 1 \text{ ns}$ were carried out for $t_d = 120 \text{ ps}$, $t_d = 160 \text{ ps}$, and $t_d = 260 \text{ ps}$.

Figure 2(a) shows the time dependences of the number of emitted electrons per time unit dN_{em}/dt and the number of emitted and generated electrons N_e for $\varphi_0 = 120 \text{ kV}$, $T = 1 \text{ ns}$, and $t_d = 160 \text{ ps}$. One can see that the EE results in a drastic increase in dN_{em}/dt at $t_d = 160 \text{ ps}$, i.e., when EE starts. The VC is formed at $t \approx 123 \text{ ps}$ [see Fig. 2(b)]. This means that the electrons that were injected just before the EE switching cannot leave the cathode-VC gap. Nevertheless, the electrons existing in region KO could become RAEs because the electric field in this region [see Fig. 2(b) and Fig. 3] reaches $E_{max} \approx 4.5 \times 10^7 \text{ V/cm}$, which is larger than the critical electric field E_{cr} for N_2 gas at atmospheric pressure ($E_{cr} = 4.5 \times 10^5 \text{ V/cm}$).³ Here, by RAEs we mean electrons with an energy larger than 1 keV. Switching EE at $t_d = 160 \text{ ps}$ leads to the injection of $dN_{em}/dt \approx 10^{11}$ electrons, which changes the potential distribution significantly [see Figs. 2(b) and 2(c)]. The electric field of EE electron space charge also accelerates the electrons existing between electrodes. In addition, the electrons that were captured in the cathode-VC gap acquire an energy larger than $e\varphi_{VC}$, and a

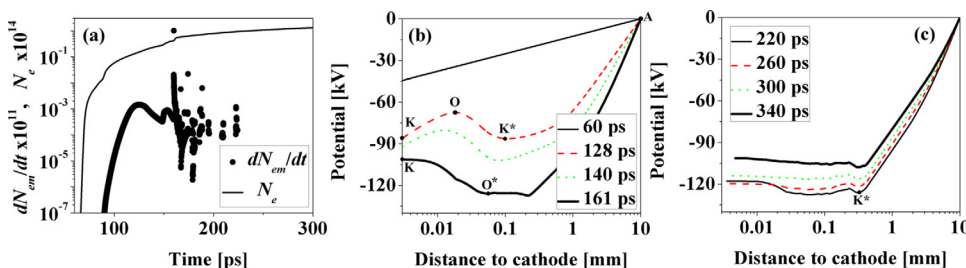


FIG. 2. (Color online) (a) Time dependence of the emitted dN_{em}/dt and total number of the electrons N_e in the CA gap. (b),(c) Potential distribution in the CA gap at different times; $\varphi_0 = 120 \text{ kV}$, $T = 1 \text{ ns}$, $t_d = 160 \text{ ps}$.

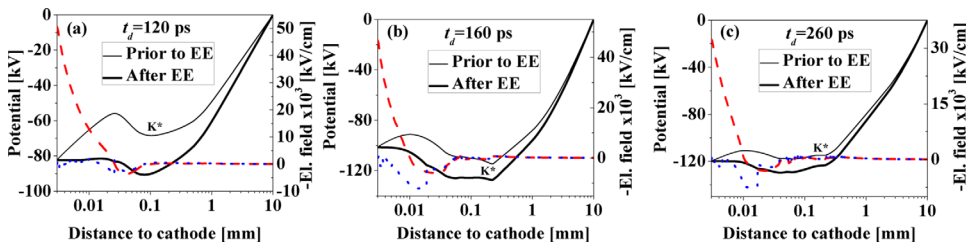


FIG. 3. (Color online) (a)–(c) Potential and electric field distributions immediately prior to and after EE turn-on for different t_d ; $\varphi_0 = 120$ kV, $T = 1$ ns. Solid lines refer to potential distribution. Dashed and dotted lines refer to electric field distribution prior to and after EE switching-on, respectively.

portion of these electrons leave the cathode-VC gap. These electrons are the electrons that are located in the VC vicinity from its cathode side.

Simulation results also showed that at some locations inside the CA gap, after the EE switching the potential is larger than the value of φ_C at that moment. In general, this could result in electrons' acquiring an energy larger than $e\Delta\varphi_{CA}$, i.e., one could obtain so-called anomalous electrons at the anode.²⁶ In earlier research²⁷ in which the transition from FE to EE was studied for a vacuum coaxial diode using PIC simulations, the generation of anomalous electrons under certain conditions was demonstrated. However, the present numerical simulations showed that in a gas-filled diode, anomalous electrons could not be obtained even for $\varphi > \varphi_C$, for three reasons. The first reason is that the electric field in most locations with $\varphi > \varphi_C$ is $E < E_{cr}$, and electrons from these locations cannot become RAEs. The second reason is that even when $E > E_{cr}$ at some locations with $\varphi > \varphi_C$, RAEs generated at these locations reach the anode with energy $e \cdot \Delta\varphi_{CA}$ because of inelastic collisions with neutrals. The third reason is the absence of RAEs in the K^* location, because the electrons existing in the KK^* region [see Fig. 2(b)] are captured in the potential well.

In addition, the turn-on of EE leads to sharp temporal variations in electron emission [see Fig. 2(a)]. This can be explained by the excess of potential inside the CA gap above $|\varphi_C|$, which causes a decrease in the potential slope at a distance from the cathode of $r \leq 0.04$ mm and leads to the termination of EE during some period of time. However, due to the continuous increase in the cathode and, thus, in the explosive plasma potential and the plasma propagation toward the anode, one obtains again a positive potential slope in the plasma boundary vicinity. The latter recovers the EE, which causes an abrupt change in the value of dN_{em}/dt [see Fig. 2(a)]. Nevertheless, newly emitted electrons cannot leave the KO^* region, and therefore these electrons do not influence RAE generation. Accumulating in the vicinity of the plasma boundary, these electrons terminate the EE again, and this process repeats until $\varphi_C = \varphi_0$.

The time of EE turn-on affects the process of RAE generation significantly. Within the time interval $0 < t < t_{VC}$, the region where the VC will be formed does not produce RAEs [see Fig. 3(a), K^* region], because at this location $E_{K^*} < E_{cr}$. During this time interval, RAEs are the electrons emitted from the cathode and generated in the cathode vicinity (at $r < 0.025$ mm). The turn-on of EE reduces significantly the electric field in the vicinity of the plasma boundary. Thus, the electrons emitted from the plasma boundary at $t > t_d$ cannot become RAEs. However, the space-charge of the EE electrons slightly increases the electric field $r \approx 0.08$ mm, thereby shifting the boundary with $E > E_{cr}$ toward the anode. For instance, when EE is turned on, one obtains $E_{K^*} \approx 5.5 \times 10^5$ V/cm, i.e., $E_{K^*} > E_{cr}$.

Figure 4(a) shows a comparison between RAE numbers N_{RAE} at different values of t_d . One can see that the EE turn-on prior to VC formation slightly reduces the value of N_{RAE} in the interval 120 ps $< t \leq t_{VC}$ ($t_{VC} = 123$ ps), because the emission from the cathode does not contribute to N_{RAE} at that time. However, at $t > 130$ ps, when the VC has been formed, the value of N_{RAE} for $t_d = 120$ ps exceeds values of N_{RAE} for $t_d = 160$ ps and $t_d = 260$ ps. This excess in N_{RAE} is composed of RAEs formed prior to the EE turn-on, the portion of the EE electrons and electrons that become RAEs due to additional acceleration by the electric field of EE electrons. In addition, Fig. 4(a) shows that the time duration of the RAE pulse is lower for $t_d = 120$ ps than for $t_d = 160$ ps and 260 ps. This can be explained by the formation of the VC. Indeed, at the t_d values of 160 ps and 260 ps, the VC is already formed, and the turn-on of EE results in a lower value of dN_{em}/dt than for the case with $t_d = 120$ ps, because of the smaller values of E at the plasma boundary (see Fig. 3). The smaller number of injected electrons leads to an insignificant change in the potential distribution at $t_d = 160$ ps and $t_d = 260$ ps in comparison with that at $t_d = 120$ ps (see Fig. 3). However, for t_d values of 160 ps and 260 ps, the VC generates RAEs prior to EE switching. Simulations showed that $E_{K^*} \approx 7.0 \times 10^5$ V/cm for $t_d = 160$ ps and $t_d = 260$ ps prior to EE turn-on, and $E_{K^*} \approx 7.5 \times 10^5$ V/cm for $t_d = 160$

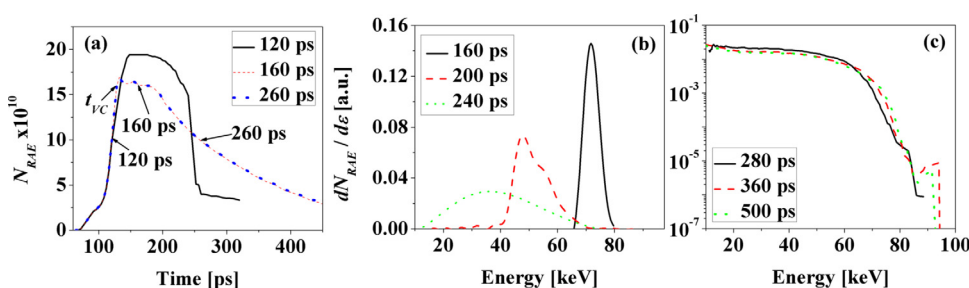


FIG. 4. (Color online) (a) RAE number (N_{RAE}) inside the CA gap at different times. (b),(c) EEDF at the anode at different times; $\varphi_0 = 120$ kV, $T = 1$ ns, $t_d = 160$ ps.

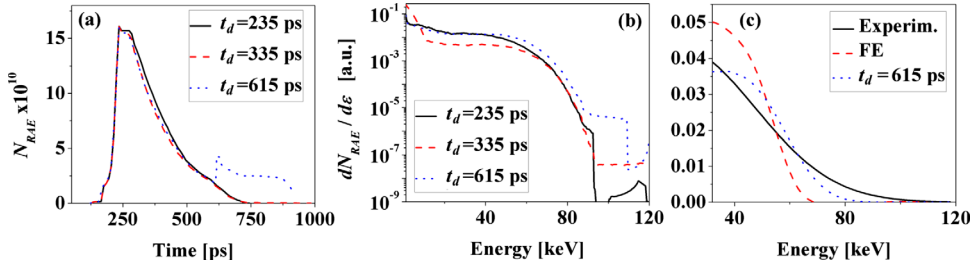


FIG. 5. (Color online) (a) RAE number (N_{RAE}) inside the CA gap at different times. (b) EEDF at the anode at different t_d at $t = T/2$. (c) Comparison between experimental (Ref. 15) and simulated EEDF; $\phi_0 = 120$ kV, $T = 2$ ns.

ps and $t_d = 260$ ps after the EE turn-on. Thus, the VC location [see Figs. 3(b) and 3(c)] at $t_d = 160$ ps and $t_d = 260$ ps contributes similarly to RAE generation prior to and after EE turn-on.

Normalized EEDFs for electrons reaching the anode with energy $\varepsilon_e \geq 1$ keV within a time interval between $t = 0$ and the considered time are shown in Figs. 4(b) and 4(c). One can see that the first electrons reaching the anode have a relatively narrow energy spectrum. Later in the accelerating pulse, the EEDF becomes broader, with the maximum of the EEDF shifting toward the lower energy. In addition, the results of simulations showed that the EEDF at $t \approx 500$ ps contains the electrons with the highest energy $\varepsilon_{emax} \approx 95$ keV [see Fig. 4(c)], despite the fact that $\phi_{K^*} > \phi_0 = 120$ kV. In fact, electrons with $\varepsilon_e \geq 100$ keV could be produced only from the VC because of electrons emitted from the cathode plasma boundary being captured in the potential well, i.e., plasma boundary VC. Indeed, the results of simulations showed that $E_{K^*} \approx 6.5 \times 10^5$ V/cm, and the electric field toward the anode decreases to E_{cr} along the distance of $\Delta r = r - r_{K^*} = 0.22$ mm. Assuming that the electron moves on average $E \approx 5.5 \times 10^5$ V/cm along Δr without any collisions, one can estimate the upper limit of the electrons' energy as $\varepsilon_e \approx 12$ keV. This energy is much lower than the energy that electrons have acquired in the cathode vicinity in the case of a non-disturbed electric field at the time when the FE begins. In addition, the value of dN_{em}/dt emitted as a result of FE is much larger than the number of electrons emitted from the VC location. These factors explain the absence of electrons with $\varepsilon_e \geq 100$ keV at the anode. Here let us note that in the case of only FE, the maximum energy of RAEs does not exceed 80 keV (see Ref. 16), i.e., the turn-on of EE leads to an increase in the maximal achievable energy of RAEs.

Now, let us consider the results of simulations for $\phi_0 = 120$ kV and $T = 2$ ns, which results in a VC being formed at time $t_{VC} \approx 215$ ps.¹⁶ Simulation results showed that EE turn-on within $t_{VC} \leq t \leq T/4$ does not significantly influence the RAE generation [see Fig. 5(a)]. However, EE turn-on at $t > T/4$ produces additional RAEs [see Fig. 5(a) for $t_d = 615$ ps]. Figure 6(a) shows the potential distribution immediately prior to and after EE turn-on, and Fig. 6(b) shows the time dependence of dN_{em}/dt . One can see that at $t \approx 615$ ps, when the electron emission from the cathode is still governed by FE, $|\phi_{K^*}| < |\phi_C|$, and only one electron is emitted during a few time steps. Therefore, the quantity of RAEs reaching the anode with $\varepsilon_e \approx e\phi_C$ is negligibly small. However, due to a large electric field ($E_{K^*} \approx 6.2 \times 10^5$ V/cm) in the region around point K^* [see Fig. 6(a)], electrons from that

location acquire an energy $\varepsilon_e > 1$ keV and become RAEs. The turn-on of EE changes the potential distribution significantly and accelerates electrons captured in the KK^* region. In addition, the simulation results showed that the value of the electric field just prior to the beginning of EE is $E_K \approx 1.7 \times 10^7$ V/cm. This leads to the acceleration of the portion of the first EE emitted electrons, which become RAEs [see the spike in the RAE current at $t_d = 615$ ps in Fig. 5(a)].

A comparison of EEDFs for different t_d is shown in Fig. 5(b). One can see that the spectra are almost identical for $\varepsilon_e < 90$ keV. However, a larger value of t_d leads to an increase in RAEs with $\varepsilon_e > 90$ keV, i.e., the time of the EE turn-on influences the EEDF high-energy tail significantly.

A comparison between the experimentally obtained EEDF (for details, see Ref. 15) and simulated EEDF at the anode, with and without EE turn-on, is presented in Fig. 5(c). The experimental spectrum was measured in air ($P = 10^5$ Pa) for $\phi_0 \approx 120$ kV, a voltage rise time of ~ 0.5 ns, and $d_{CA} = 1$ cm. One can see that simulated spectra agree better with experimental spectra when EE is included in the simulation. Both the simulation and experimental EEDFs show that only a small portion of the electrons have energies $\varepsilon_e \sim e\phi_C$, whereas the majority of the electrons have energies $\varepsilon_e < 40$ keV. In addition, it is important to note that the EE turn-on increases N_{RAE} with $\varepsilon_e > 60$ keV as compared with the case in which the electron emission is governed only by FE.

IV. SUMMARY

Numerical simulations of the generation of RAEs in a N_2 -gas-filled coaxial diode with a cathode operating in field emission that transfers to explosive emission were carried out using the 1D PIC numerical code. It was shown that the time of EE turn-on significantly influences the generation of RAEs. Namely, when the turn-on of EE occurs prior to the VC formation, the EE electrons screen the electric field in the cathode vicinity. This leads to the termination of the

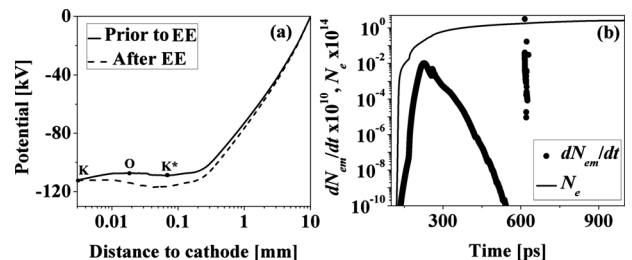


FIG. 6. (a) Potential distribution immediately before and after EE turn-on. (b) Time dependence of dN_{em}/dt and N_e ; $\phi_0 = 120$ kV, $T = 2$ ns, $t_d = 615$ ps.

generation of RAEs that consist of electrons being emitted by FE and existing in the cathode vicinity. Concerning EE electrons, only the electrons emitted during the first few picoseconds after the EE was turned on become RAEs and contribute significantly to the RAE current. This leads to an increase in the amplitude of the RAE current and a decrease in its duration.

EE turn-on after the VC formation and during the HV rise time does not significantly influence RAE generation. Simulations have shown that the VC can be considered as a major source of RAEs prior to and after EE turn-on, and therefore EE does not influence RAE generation. In this case, an increase in the value of t_d leads only to an insignificant increase in the number of RAEs. In addition, it was shown that EE turn-on during the HV fall (and after the VC formation) leads to additional RAE generation.

A comparison of EEDFs obtained with and without EE turn-on has shown that the former increases the number of electrons in the high-energy tail of the EEDF and the electrons' largest energy. A comparison of simulated EEDFs with the experimentally obtained electron spectrum has shown the best fit when the EE turn-on is considered in simulations.

ACKNOWLEDGMENTS

This work was supported in part at Technion by a fellowship from the Lady Davis Foundation and by the Center for Absorption in Science, Ministry of Immigrant Absorption, State of Israel.

¹S. M. Starikovskaya, *J. Phys. D: Appl. Phys.* **39**, R265 (2006).

²G. A. Mesyats, V. V. Osipov, and V. F. Tarasenko, *Pulsed Gas Laser* (SPIE, Bellingham, WA, 1995).

³G. A. Mesyats, M. I. Yalandin, K. A. Sharypov, V. G. Shpak, and S. A. Shunailov, *IEEE Trans. Plasma Sci.* **36**, 2497 (2008).

⁴L. M. Vasilyak, S. V. Kostyuchenko, N. N. Kudryavtsev, and I. V. Filyugin, *Phys. Usp.* **27**, 247 (1994).

⁵O. A. Sinkevich and Yu. V. Trofimov, *High Temp.* **18**, 1088 (1980) (in Russian).

⁶B. B. Slavin and P. I. Sopin, *High Temp.* **30**, 1 (1992) (in Russian).

⁷O. V. Boutine, S. V. Kostyoutchenko, A. V. Krasnochub, and L. M. Vasilyak, *J. Phys. D: Appl. Phys.* **33**, 791 (2000).

⁸S. M. Starikovskaia and A. Yu. Starikovskii, *J. Phys. D: Appl. Phys.* **34**, 3391 (2001).

⁹E. E. Kunhardt, Y. Tzeng, and J. P. Boeuf, *Phys. Rev. A* **34**, 440 (1986).

¹⁰L. P. Babich, *High-Energy Phenomena in Electric Discharges* (Futurepast, Arlington, VA, 2003).

¹¹G. A. Mesyats and M. I. Yalandin, *IEEE Trans. Plasma Sci.* **37**, 785 (2009).

¹²V. F. Tarasenko and S. I. Yakovlenko, *Phys. Usp.* **47**, 887 (2004) and references therein.

¹³V. A. Shklyaev and V. V. Ryzhov, *Tech. Phys. Lett.* **37**, 72 (2011) and references therein.

¹⁴M. I. Yalandin, G. A. Mesyats, A. G. Reutova, K. A. Sharypov, V. G. Shpak, and S. A. Shunailov, *Tech. Phys. Lett.* **37**, 371 (2011).

¹⁵S. Yatom, V. Vekselman, J. Z. Gleizer, and Ya. E. Krasik, *J. Appl. Phys.* **109**, 073312 (2011).

¹⁶D. Levko, S. Yatom, V. Vekselman, J. Z. Gleizer, V. Tz. Gurovich, and Ya. E. Krasik, *J. Appl. Phys.* **111**, 013303 (2011).

¹⁷C. K. Birdsall and A. B. Langdon, *Plasma Physics via Computer Simulation* (IoP Publishing, Bristol, UK, 1991).

¹⁸See <http://physics.nist.gov/PhysRefData/Ionization/Xsection.html> for the NIST Electron-Impact Cross Section Database.

¹⁹Y. Itikawa, *J. Phys. Chem. Ref. Data* **35**, 31 (2006).

²⁰M. Surendra, D. B. Graves, and I. J. Morey, *Appl. Phys. Lett.* **56**, 1022 (1990).

²¹Compilation of electron cross sections used by A. V. Phelps, http://jila.colorado.edu/~avp/collision_data/electronneutral/ELECTRON.TXT.

²²A. Okhrimovskyy, A. Bogaerts, and R. Gijbels, *Phys. Rev. E* **65**, 037402 (2002).

²³Yu. P. Raizer, *Gas Discharge Physics* (Springer, Berlin, 1991).

²⁴G. A. Mesyats, *JETP Lett.* **85**, 109 (2007).

²⁵E. A. Litvinov, G. A. Mesyats, and D. I. Proskurovskii, *Phys. Usp.* **26**, 138 (1983).

²⁶L. P. Babich, T. V. Loiko, and V. A. Tsukerman, *Phys. Usp.* **33**, 521 (1990).

²⁷D. Levko, V. Tz. Gurovich, and Ya. E. Krasik, *J. Appl. Phys.* **110**, 043302 (2011).